

Single-Cell Enzyme Concentrations, Kinetics, and Inhibition Analysis Using High-Density Hydrodynamic Cell Isolation Arrays

Dino Di Carlo, Nima Aghdam, and Luke P. Lee*

Biomolecular Nanotechnology Center, Berkeley Sensor and Actuator Center, Department of Bioengineering, University of California, Berkeley, California 94720

High-quality single-cell data are required for a quantitative systems biology description of cellular function. However, data of this type are difficult and time-consuming to collect using traditional techniques. We present a robust and simple microfluidic method for trapping single cells in large arrays to address this problem. Ordered single-cell isolation arrays allow for high-density microscopic analysis with simplified image processing. Moreover, for fluorescent assays, on-chip sample preparation (e.g., fluorescent labeling, washing) can be performed, as opposed to manual intensive operations of incubation, centrifugation, and resuspension in previous techniques—saving time and reagents. This technology was applied to determine novel single-cell enzyme kinetics for three different cell types (HeLa, 293T, Jurkat). A kinetic model of this process predicted this varied response was due to variation in the concentration of carboxylesterase between cell types. Nordihydroguaiaretic acid (NDGA) was also characterized as an inhibitor of carboxylesterases. For HeLa cells, 20 nM of the 50 nM total carboxylesterases was unaffected by NDGA. This type of analysis could be directly applied to quantify a variety of intracellular enzymes with available fluorogenic substrates.

It has recently been shown that genetically identical cells have large variation in observed gene expression and behavior.^{1,2} This is largely due to temporal and spatial stochasticity in the underlying chemical processes. Thus, statistically rich single-cell data from a large number of cells are required to obtain a useful distribution of the possible chemical states that a cell can occupy. Bulk experiments fall short of providing adequate data in that the results elucidate the mean value of a parameter with further experiments providing information about the standard error of the mean. In contrast, single-cell experiments reveal the critical underlying distribution of parameters. This contrast is especially apparent in time-dependent processes in which by averaging over a population a smooth transition is observed from one state to another, obscuring the underlying transition occurring at the single-cell level, which may occur in a stepwise manner.³

There are various reported methods to collect single-cell data in a high-throughput manner. The most common techniques are flow cytometry (FC),^{4,5} laser scanning cytometry (LSC),⁶ and automated microscopy.⁷ In determining enzyme concentrations within individual cells, requirements include continuous monitoring of fluorescence levels in individual cells as well as a known cell volume. FC is unable to monitor the same cell at multiple time points while LSC and automated microscopy techniques require knowledge of cell volume in nonspherical cells or methods to immobilize spherical cells. Additionally, in the latter two techniques, a nonuniform distribution of cell positions complicates image analysis.

Microfluidic approaches have been developed to allow more precise control of cell positioning and reagent introduction in analyzing single cells.^{8–13} Also noteworthy is work using U-shaped weirs to isolate single cells by observing and controlling the flow during the experiment.^{14,15} Implementations of these methods for large-scale single-cell analysis is still in progress. Complementary techniques to form large regular arrays of single cells have also been reported.^{2,16–20} Poly(dimethylsiloxane) (PDMS) well arrays on a substrate allow dense positioning of cells, but drawbacks include nonuniform exposure of reagents to trapped cells, with

- (4) Martin, J. C.; Swartzendruber, D. E. *Science* **1980**, *207*, 199–201.
- (5) Nolan, J. P.; Sklar, L. A. *Nat. Biotechnol.* **1998**, *16*, 633–638.
- (6) Griffin, S.; Taggart, C. C.; Greene, C. M.; O'Neill, S.; McElvaney, N. G. *FEBS Lett.* **2003**, *546*, 233–236.
- (7) Perlman, Z. E.; Slack, M. D.; Feng, Y.; Mitchison, T. J.; Wu, L. F.; Altschuler, S. J. *Science* **2004**, *306*, 1194–1198.
- (8) Wheeler, A. R.; Thronset, W. R.; Whelan, R. J.; Leach, A. M.; Zare, R. N.; Liao, Y. H.; Farrell, K.; Manger, I. D.; Daridon, A. *Anal. Chem.* **2003**, *75*, 3581–3586.
- (9) Yang, M. S.; Li, C. W.; Yang, J. *Anal. Chem.* **2002**, *74*, 3991–4001.
- (10) Voldman, J.; Gray, M. L.; Toner, M.; Schmidt, M. A. *Anal. Chem.* **2002**, *74*, 3984–3990.
- (11) Peng, X. Y.; Li, P. C. H. *Anal. Chem.* **2004**, *76*, 5273–5281.
- (12) Seger, U.; Gawad, S.; Johann, R.; Bertsch, A.; Renaud, P. *Lab Chip* **2004**, *4*, 148–151.
- (13) Wu, H. K.; Wheeler, A.; Zare, R. N. *Proc. Natl. Acad. Sci. U.S.A.* **2004**, *101*, 12809–12813.
- (14) Li, P. C. H.; de Camprieu, L.; Cai, J.; Sangar, M. *Lab Chip* **2004**, *4*, 174–180.
- (15) Li, X. J.; Li, P. C. H. *Anal. Chem.* **2005**, *77*, 4315–4322.
- (16) Tanase, M.; Felton, E. J.; Gray, D. S.; Hultgren, A.; Chen, C. S.; Reich, D. H. *Lab Chip* **2005**, *5*, 598–605.
- (17) Rettig, J. R.; Folch, A. *Anal. Chem.* **2005**, *77*, 5628–5634.
- (18) Chin, V. I.; Taupin, P.; Sanga, S.; Scheel, J.; Gage, F. H.; Bhatia, S. N. *Biotechnol. Bioeng.* **2004**, *88*, 399–415.
- (19) Revzin, A.; Sekine, K.; Sin, A.; Tompkins, R. G.; Toner, M. *Lab Chip* **2005**, *5*, 30–37.
- (20) Taff, B. M.; Voldman, J. *Anal. Chem.* **2005**, *77*, 7976–7983.

* To whom correspondence should be addressed. E-mail: lplee@socrates.berkeley.edu.

(1) Rao, C. V.; Wolf, D. M.; Arkin, A. P. *Nature* **2002**, *420*, 231–237.

(2) Kuang, Y.; Biran, I.; Walt, D. R. *Anal. Chem.* **2004**, *76*, 6282–6286.

(3) Lidstrom, M. E.; Meldrum, D. R. *Nat. Rev. Microbiol.* **2003**, *1*, 158–164.

diffusion into the well. Holographic optical trapping methods were not used because for the longer (10–40 min) studies heating of the cells and surrounding fluid may lead to cell death.²¹ Dielectrophoretic trapping arrays although allowing more control of cell positioning and release require additional electrical connections and more complicated fabrication than purely microfluidic approaches.^{10,20}

We report a comprehensive technology in which high-density regular arrays of single cells are isolated in a purely hydrodynamic fashion within a microfluidic device—allowing uniform convective reagent control and reduced image processing. Cell loading is quick (<30 s) and easy to perform. Using this technology, we report novel data on the single-cell concentration distribution of carboxylesterases within three different human cell lines, as well as on the inhibition of intracellular esterases by the nonspecific inhibitor nordihydroguaiaretic acid (NDGA). These types of analyses are enabled by interrogating spherical suspended cells with known volumes as opposed to adherent cells.

Various carboxylesterases, along with having essential biochemical functions (ester and amide hydrolysis), may activate prodrugs and contribute to inactivation of other pharmaceuticals.²² Thus, understanding the variation in carboxylesterase expression levels between individuals will be important in tailoring personalized pharmacological interventions. Carboxylesterase extracts have been shown to be inhibited by NDGA *in vitro*;²³ however, no studies have investigated the inhibition of intracellular carboxylesterases or the fraction of intracellular esterases that is uninhibited. The effect of carboxylesterase inhibition by NDGA and its relation to anticancer,²⁴ antiviral,²⁵ and general inflammation-modulating²⁶ properties of the compound are unknown.

EXPERIMENTAL METHODS

Microfluidic Chip Fabrication. The molds for the microfluidic channels and hydrodynamic trapping arrays were fabricated using negative photoresists (SU-8 50 and SU-8 2002, Microchem Corp., 3000 rpm spin speed, 40 and 2 μm thick). Details of the mold fabrication are shown in Figure S-1 (Supporting Information). Rounded trap geometries were created by increasing the manufacturer-specified exposure energy by 60%. PDMS (Sylgard 184, Dow Corning) was prepared according to the manufacturer's instructions, degassed in a vacuum chamber for 1 h, and then poured on the mold and cured in a 70 °C oven for 6 h. The PDMS was then carefully peeled off the mold. The fluid inlet and outlet were punched by a flat-tip needle for tube connections. Both a glass slide and the PDMS structures were treated with oxygen plasma (2 Torr, 40 W) for 40 s before bonding.

Cell Culture and Preparation. HeLa (human cervical carcinoma), Jurkat (human T-cell leukemia), and 293T (human embryonic kidney, HEK) immortalized cell lines were used in experiments (American Type Culture Collection, Bethesda, MD).

(21) Neuman, K. C.; Chadd, E. H.; Liou, G. F.; Bergman, K.; Block, S. M. *Biophys. J.* **1999**, *77*, 2856–2863.

(22) Satoh, T.; Hosokawa, M. *Annu. Rev. Pharmacol. Toxicol.* **1998**, *38*, 257–288.

(23) Schegg, K. M.; Welch, W. *Biochim. Biophys. Acta* **1984**, *788*, 167–180.

(24) Soriano, A. F.; Helfrich, B.; Chan, D. C.; Heasley, L. E.; Bunn, P. A.; Chou, T. C. *Cancer Res.* **1999**, *59*, 6178–6184.

(25) Gnable, J. N.; Brady, J. N.; Clanton, D. J.; Ito, Y.; Dittmer, J.; Bates, R. B.; Huang, R. C. C. *Proc. Natl. Acad. Sci. U.S.A.* **1995**, *92*, 11239–11243.

(26) van Puijenbroek, A. A. F. L.; Wissink, S.; van der Saag, P. T.; Peppelenbosch, M. P. *Cytokine* **1999**, *11*, 104–110.

The cells were maintained by passaging twice weekly with Dubelcco's modified Eagle medium (DMEM) for adherent cells or RPMI 1640 for suspension cells supplemented with 10% fetal bovine serum (FBS). For a typical enzyme concentration experiment on chip, adherent cells were detached from one confluent 100-mm diameter culture dish with 2 mL of trypsin EDTA (0.25%, Gibco, Carlsbad, CA). An equal amount of DMEM + FBS was then added to deactivate remaining trypsin. Cells were then centrifuged to a pellet and resuspended in phosphate-buffered saline pH 7.4 (PBS, Gibco). A key experimental detail is to trap suspended cells within 15 min of trypsinization to reduced nonspecific adhesion to surfaces. However, no chemical modification of the surface was performed. For Jurkat cells, a fraction of suspended cells was diluted with PBS and loaded directly into the device. It was noted that Jurkat cell adhesion to device surfaces was much less than for the adherent cell lines, and a constant flow was required to maintain all cells within traps. Freshly suspended cells were introduced into previously PBS-filled devices by a syringe connected to a three-way valve.

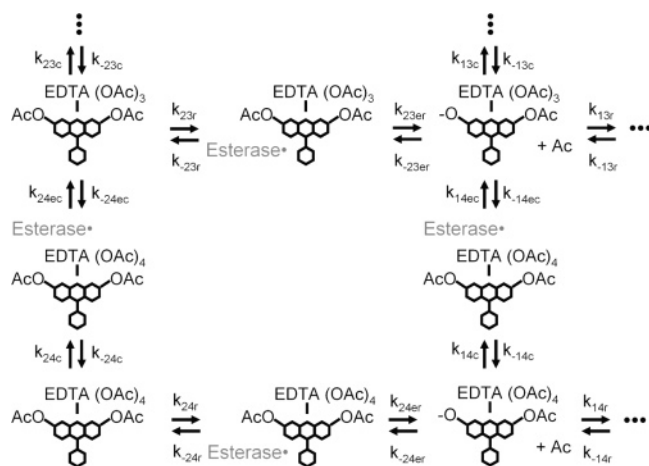
Assay of Single-Cell Enzyme Kinetics. Experiments to determine enzyme concentrations and kinetics were conducted using two different techniques. In the first technique, a cell type was introduced into the isolation arrays by syringe and washed, followed by introduction of 3 μM calcein AM solution via syringe pump at a flow rate of 20 $\mu\text{L min}^{-1}$ (average velocity near cells $\sim 30 \mu\text{m s}^{-1}$). The device was mounted on the stage of a Nikon Eclipse TS100 microscope. Excitation light from a mercury arc lamp was filtered with a FITC filter set focused through a 10 \times objective (0.25 NA, 8.5- μm depth of field), and emitted light was collected using the same objective, filtered, and imaged onto the CCD of a cooled camera (Cascade: 512B, Roper Scientific, Tucson, AZ). Images (1-s exposure) were acquired at 10-s intervals.

In a second technique, using the same detection setup, a cell type was loaded into approximately half of the available traps, washed, and an image was taken. Next, the other cell type was introduced into the remaining traps, washed, and imaged. In this way, 3 μM calcein AM (20 $\mu\text{L min}^{-1}$) was introduced to both cells in identical environments and data for each cell type could be isolated. This was used as a control for device-to-device variation. These data were compared to data on the same cells obtained using separate devices at separate times to check repeatability. All data sets, not varying more than a standard deviation within the same cell type, were combined in the data shown in Figure 3.

Intracellular Carboxylesterase Inhibition by NDGA. To assay inhibition of carboxylesterases, NDGA (0.5 nM–120 μM) (Sigma Aldrich, St. Louis, MO) was combined with 3 μM calcein AM and introduced into the cell isolation array loaded with HeLa cells as discussed above for kinetic assays. Additionally, the microscope and light sources were set up in the same configurations as described above. Intensity data were collected from the Cascade:512B cooled CCD at 10-s intervals with a 1-s exposure time.

Data Collection and Control Experiments. Intensity data from the Cascade:512B was stored with 16-bit gray scale levels in multipage tif format using WinView (Roper Scientific, Tucson, AZ). Single-cell intensity data were then analyzed using a custom Matlab (The MathWorks, Natick, MA) script to extract cell

Scheme 1. Calcein AM Cleavage Reaction Network



intensity and geometric parameters. Because of the predetermined arrangement of trapped single cells, the processing script only requires one set of position data to find all individual cells in the array; no cell identification code is required. Intensities were cell volume normalized, which leads to a much narrower distribution of responses as opposed to reporting total cell intensity. All data were corrected for bleaching by preloading calcein AM-dyed cells and measuring volume-normalized intensity decrease with time, using the same microscope setup. Bleaching data were fit with an exponential ($dI/dt = -kI$), and k was extracted to correct all other data. After correcting for bleaching, volume-normalized intensity data were converted to concentration of calcein by determining volume-normalized intensity for a solution of 1 μM calcein introduced into the device with identical microscope parameters (Figure S-2, Supporting Information). To determine that the mapping from intensity to concentration was linear, the intensities yielded by a range of calcein concentrations (1–20 μM) were measured (Figure S-3, Supporting Information). The R^2 for a linear fit to the data was 0.99. Figure S-4 (Supporting Information) shows data from HeLa and 293T cells before and after volume normalization, bleach correction, and conversion to calcein concentration.

Kinetic Analysis. Fluorescent intensity data were interpreted using a novel kinetic model of calcein AM ester hydrolysis catalyzed by intracellular carboxylesterases (Scheme 1). In this situation, there are six possible ester cleavage sites, with cleavage of the ring sites resulting in fluorescence. Cleavage of one ring acetate results in a ~ 30 times less fluorescent molecule than cleavage of both ring acetates.²⁷ The kinetics of the entire matrix of possible cleavage steps in various sequences was modeled computationally using a Matlab script (code S-5,6). Here the concentration of each chemical species was stored at each time step. Diffusion of calcein AM into the cell as well as diffusion of monocharged compounds out of the cell was accounted for in the code. Membrane diffusion constants for calcein AM and calcein AM monoion derivatives were optimized starting with previously determined diffusion constants for fluorescein diacetate (FDA) and 6-carboxy-FDA (1.7×10^{-15} and $7.8 \times 10^{-17} \text{ m}^2 \text{ s}^{-1}$, respectively).²⁸ For calcein AM, a much larger molecule, the diffusion

(27) Hofmann, J.; Sernetz, M. *Anal. Biochem.* **1983**, *22*, 180–186.

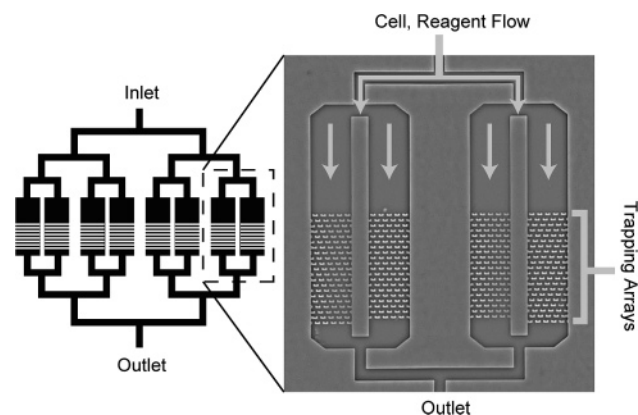


Figure 1. Microfluidic single-cell isolation arrays. A schematic diagram of the overall microfluidic device is shown. Branching delivery channels ensure more equal distribution of flow with cells and reagents to each trapping array. Only one inlet and outlet are needed, since solutions of cells and reagents are easily switched with an off-chip valve. The inset shows more details of the device in a micrograph of a pair of trapping arrays.

constants had to be decreased in both cases to correctly predict the intensity line shape (5.0×10^{-16} and $9.0 \times 10^{-20} \text{ m}^2 \text{ s}^{-1}$, respectively). Kinetic constants were then constrained by both literature values and best fits to data sets for HeLa and 293T intensity data with only variation in enzyme concentration allowed between data sets. Additionally, for simplicity, cleavage or binding reactions at different calcein AM binding sites were considered to have the same kinetic constants irrespective of sterics or charge. All kinetic constants are listed in Table S-1 (Supporting Information). Initial acetate levels were taken to be similar to measured plasma acetate levels (18–48 μM).^{29,30} Diffusion of acetate from the cell was not taken into account due to cell sequestering mechanisms in the form of acetyl-CoA.³¹

RESULTS

Single Cells Are Isolated in High-Density Arrays. Cells were introduced through a branching introduction channel of replica molded PDMS devices to individual trapping arrays (Figure 1). Only one trapping array was observed over the duration of an experiment. Single cells were isolated in regular high-density arrays composed of two channel height levels. The larger 40- μm channel height served as the main fluid conduits for cell solutions, while the 2- μm -height regions were used to form elevated trapping regions (Figure 2a). Having a 2- μm gap allows a fraction of fluid streamlines carrying cells to enter a trap. Once a cell enters a trap and partially occludes the 2- μm gap, the fraction of fluid streamlines (and cells) entering the trap region is reduced. This leads to a high quantity of single-cell isolates (Figure 2b, Figure 3a,e). In effect, the probability of trapping is dependent on the number of cells previously trapped. This is shown statistically, by comparing a Poisson distribution to the experimentally measured distribution in Figure 3e ($N = 199$ trapping sites, 4

(28) Breeuwer, P.; Drocourt, J. L.; Bunschoten, N.; Zwietering, M. H.; Rombouts, F. M.; Abee, T. *Appl. Environ. Microbiol.* **1995**, *61*, 1614–1619.

(29) Naoum, H.; Van Nes, J. J.; Kappert, H. J.; Beynen, A. C. *J. Anim. Physiol. Anim. Nutr.* **2002**, *86*, 105–110.

(30) Scheppach, W.; Pomare, E. W.; Elia, M.; Cummings, J. H. *Clin. Sci.* **1991**, *80*, 177–182.

(31) Wolfe, A. J. *Microbiol. Mol. Biol. Rev.* **2005**, *69*, 12.

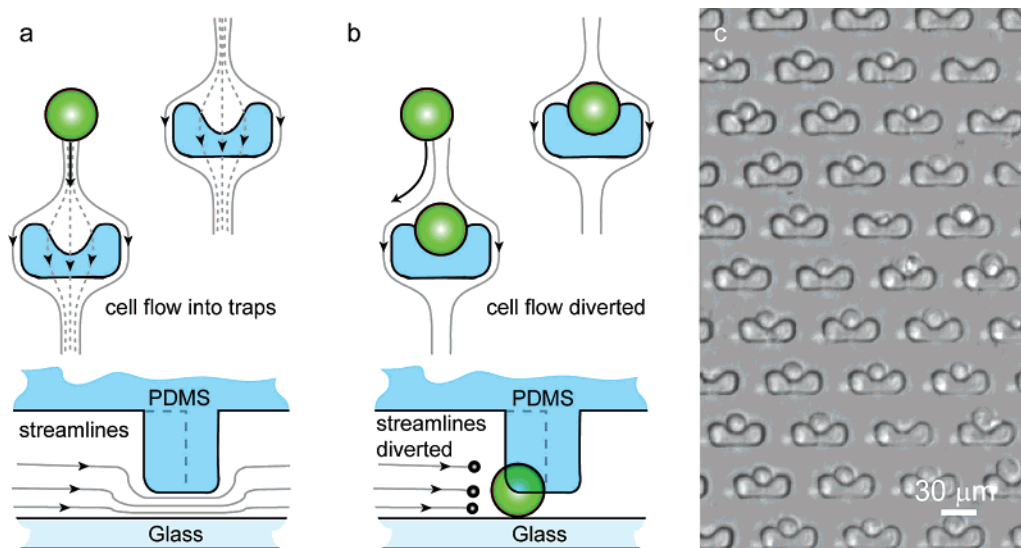


Figure 2. High-density single-cell isolation. (a,b) A schematic diagram is shown to describe the mechanism of cell trapping using flow-through arrayed suspended obstacles. Two-layer (40 and 2 μm) cup-shaped PDMS trapping sites allow a fraction of fluid streamlines to enter the traps. After a cell is trapped and partially occludes the 2- μm open region, the fraction of streamlines through the barred trap decreases, leading to the self-sealing quality of the traps and a high quantity of single-cell isolates. Drawing is not to scale. (c) A phase contrast image of an array of single trapped cells is shown. The scale bar is 30 μm .

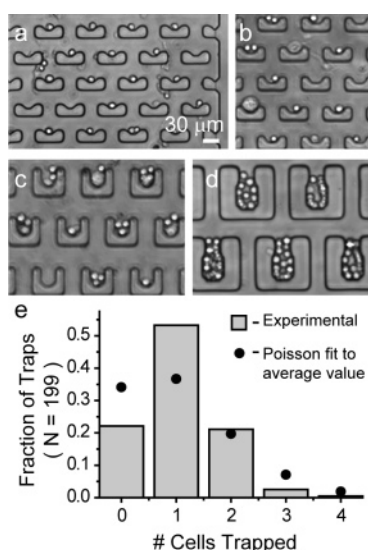


Figure 3. Statistics of single-cell isolation (a–d) Phase contrast micrographs of cell trapping in varying geometry cell isolation traps are shown. From (a) to (d), trap depth varied as 10, 15, 30, and 60 μm . The number of cells trapped scales with the trap size, with more trapping of single cells observed as the trap size decreases. (e) The distribution of trapped cells for the geometry shown in (a) is plotted along with a Poisson distribution for the same average value. If the probability of trapping was independent of the amount of previously trapped cells, one would expect a Poisson distribution. In this case, an enhancement of single-cell-containing traps and a reduction of zero and greater than two cell-containing traps is observed above the random process. Here data from four separate loadings of 100 μL of cell solution containing $\sim 3 \times 10^6$ cells mL^{-1} flowed through the device before data were collected.

separate loadings). If trapping were independent of the previous trapping events the data should follow a Poisson distribution. Here single cells are shown in excess of the Poisson distribution while zero, three, and four trapped cells are depressed. If one tries to explain trapping to be purely dependent on geometrical fit, then

trapping of two cells is expected to be more common since the channel height is more than double the diameter of the typical mammalian cell (40 μm compared to 15 μm).

Various trap sizes were investigated to achieve a high fraction of single-cell isolates. Maintaining the same trap width and channel height, the depth of the traps was varied from 10 to 60 μm . The depth of the trapping structures, signifying the “deepness” of the pocket, should not be confused with the channel depth, which we are referring to as “height” in this description. These various depths resulted in large differences in the number of trapped cells (Figure 3). For the 10- μm -deep traps, > 50% of traps contained single cells, with a decreasing fraction of single-cell isolates as trap depth increased. The distribution of number of cells trapped for the 10- μm -deep traps is shown in Figure 3e.

Devices were found to be quite effective and easy to use, with trapping able to be conducted in less than 30 s. Also, demonstrating the robustness of the method, the device has been successfully fabricated and operated by five colleagues, including undergraduate students, after minimal training.

Carboxylesterase Distributions for HeLa, Jurkat, and 293T Cell Lines. Using the 10- μm -deep trap arrays, experiments were conducted to elucidate the kinetics and concentrations of intracellular carboxylesterases in HeLa, Jurkat, and 293T cells lines (See Experimental Methods). Various carboxylesterases, along with having essential biochemical functions (ester and amide hydrolysis), may activate prodrugs and contribute to inactivation of other pharmaceuticals.²² A combined kinetic–diffusion model was developed to interpret intensity changes due to the intracellular activation of the fluorogenic substrate calcein AM (Scheme 1, code S-5,6). To simplify the parameter space, the kinetic constants for each acetate cleavage step were considered equal, irrespective of total molecule charge or steric considerations. Kinetic parameters were then fitted, bounded by literature data for related substrates and enzymes.^{27,32} The fitted kinetic param-

(32) Fiedler, F.; Hinz, H. *Eur. J. Biochem.* **1994**, *33*, 75–81.

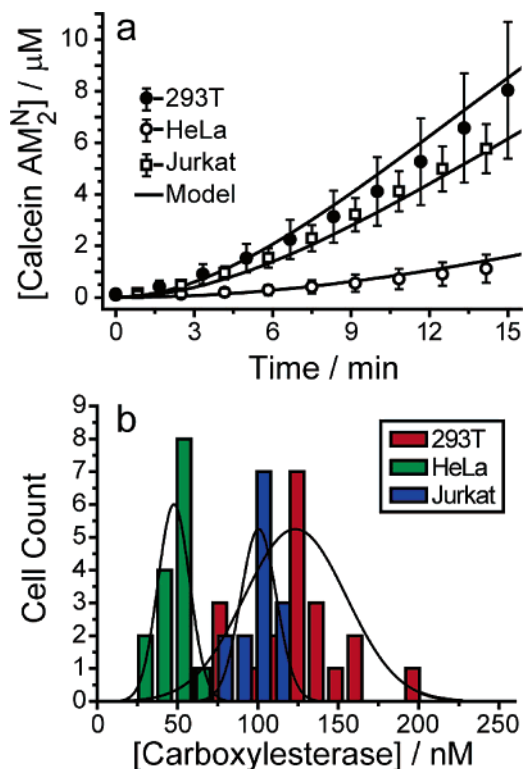


Figure 4. Single-cell array enzymology. (a) For the average of a number of single 293T (closed circles), HeLa cells (open circles), and Jurkat cells (open squares), the amount of calcein AM converted to fluorescent product is plotted as a function of time. Error bars represent plus and minus one standard deviation. The model predictions with best-fit intracellular carboxylesterase concentrations are also plotted (solid line). The average amount of carboxylesterase for 293T cells was 123 ± 32 nM ($N = 21$) and for Jurkat cells was 100 ± 11 nM ($N = 14$), while for HeLa cells it was much lower: 47.7 ± 9.5 nM ($N = 15$). (b) A histogram of the predicted enzyme concentrations for 293T, Jurkat, and HeLa cells is shown with Gaussian fits.

eters along with the sensitivity of the parameters are compiled in Table S-1. It should be noted that all kinetic parameters are for the ensemble response of the various carboxylesterases and their isozymes (hydrolases, thioesterases).²²

With this reduced-complexity model, using the average cell response, the best fits for carboxylesterase concentration yielded a concentration of 48 nM for HeLa cells, 100 nM for Jurkat cells, and 123 nM for 293T cells (Figure 4a). Fitting each individual cell response yielded a histogram of the carboxylesterase distribution for these cell types (Figure 4b). Interestingly, kidney-derived 293T cells had a larger range of enzyme concentrations when compared to both Jurkat and HeLa cell lines. For a cell diameter of ~ 10 μm, the effective concentrations of enzyme determined correspond to ~ 3000 – 7500 active sites/cell.

NDGA Inhibits a Fraction of Intracellular Carboxylesterases. Inhibition of intracellular carboxylesterases can lead to interactions with various esterase-activated or degraded pharmaceuticals. We investigated inhibition by NDGA, a lignan of the creosote bush of the southwestern United States. In these experiments, isolated single-cell arrays with trapped HeLa cells were exposed to a range of concentrations of NDGA from 0.5 nM to 120 μM, along with calcein AM. Intensity data were then collected and interpreted with the kinetic model that was modified to include a competitive inhibitor (assuming NDGA inhibits at

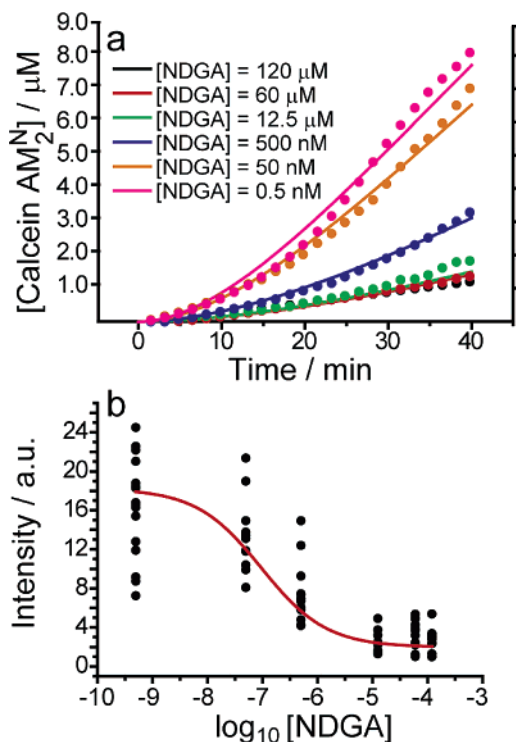


Figure 5. Inhibitor analysis at the single-cell level. (a) The time course of intracellular fluorescent activated calcein AM concentrations are plotted for varying concentrations of the nonspecific inhibitor NDGA. Data (solid circles) are average data from 9 to 15 individual cells. Modeling results with NDGA included as a competitive inhibitor are also plotted as solid lines. The data over all NDGA concentrations are fit best with an IC_{50} of 233 nM. The model also predicts that 40% of intracellular carboxylesterases are not inhibited by NDGA. (b) Dose–response plot for NDGA inhibition. Each data point corresponds to an individual cell.

the active site of the enzymes). The average data ($N = 9$ – 15 HeLa cells per NDGA concentration) and best model fits (Figure 5a) yielded a K_i or IC_{50} of 233 nM. An additional result obtained from the modeling was that 20 nM of the 50 nM effective concentration of carboxylesterase in HeLa cells was not inhibited by NDGA. The range in the single-cell inhibition data is observed in Figure 5b. The intensity for individual cells (black circles) is plotted after 40 min of enzyme activity in the presence of varying concentrations of NDGA. A less correct (since intensity is not linearly related to enzyme activity) but more commonly performed sigmoid fit to these data reveals an IC_{50} of 95 nM.

DISCUSSION

We have demonstrated a novel and robust method to obtain high-quality, parallel, single-cell data. Differences in this method when compared to other fluid mechanical methods of trapping^{8,9} include “self-sealing” of the trap as the resistance increases, geometrical tuning to enhance single-cell isolates with a simple flow through procedure, and high-density arrayability. Using this method, we present novel data on intracellular carboxylesterase (and isozyme) concentration within three human cell lines. NDGA inhibition of intracellular carboxylesterases was also measured, and it was found to inhibit $\sim 60\%$ of this enzyme activity.

Previously, kinetic models for esterase cleavage of the related fluorogenic compound fluorescein diacetate have been reported

(not in live cells); however, no attempts have been made to understand the kinetic behavior of cleavage for calcein AM (a more complex molecule, with 6 cleavage sites). Using our kinetic model for calcein AM conversion yielded similar kinetic constants in most cases (Table S-1); however, a notable difference is in the Michaelis–Menten assumptions that were used previously and not used here. Previously, kinetic measurements were not performed in whole cells.^{27,28} Here we obtain the integrated kinetic behavior of various carboxylesterase isozymes, both membrane-bound and cytosolic in their native environment. Using this model, it was found that the kidney cell line 293T had higher levels of carboxylesterases than found in the epithelial-derived HeLa line. This agrees with previous reports of moderate levels of carboxylesterase in rat kidney proximal tubule cells.²² However, concentrations were not available in the literature for comparison.

The kinetic model could be improved by considering different kinetic constants for binding and cleavage at different sites on the substrate molecule due to steric interactions. Additionally, substrates with different charge may have different constants due to electrostatic interactions influencing the transition-state energy levels. Finally, the varied carboxylesterase isozymes will have a range of kinetic parameters that when included may increase accuracy of predictions. To arrive at a unique solution with this greatly increased parameter set would require more experimentation on different aspects of the system (i.e., slightly different substrates with extra charge/sterics, isolation of particular isozymes, etc.). However, in terms of a lumped carboxylesterase response, and the ability to extract some quantitative data on carboxylesterase concentration, we argue that the current analysis is sufficient. This type of analysis may also be applied to a variety of other membrane-permeable fluorogenic substrates that target various enzymes.³³ Particularly encouraging is the recent work toward developing a variety of fluorescein-derived, membrane-permeable probes targeting a variety of intracellular enzymes.³⁴

NDGA was found to inhibit ~60% of carboxylesterases with an IC_{50} of 233 nM, much lower than that reported for inhibition of lung cancer cell growth (IC_{50} 10–60 μ M).²⁴ This suggests one possible mechanism for NDGA action in limiting cancer cell growth; additionally, synergistic effects with other cancer drugs may be observed if degradation pathways for that drug involve carboxylesterases. Negative effects would be observed for cancer prodrugs activated by carboxylesterases such as Irinotecan.³⁵

(33) Boonacker, E.; Van Noorden, C. J. F. *J. Histochem. Cytochem.* **2001**, *49*, 1473–1486.

(34) Urano, Y.; Kamiya, M.; Kanda, K.; Ueno, T.; Hirose, K.; Nagano, T. *J. Am. Chem. Soc.* **2005**, *127*, 4888–4894.

(35) Bencharit, S.; Morton, C. L.; Howard-Williams, E. L.; Danks, M. K.; Potter, P. M.; Redinbo, M. R. *Nat. Struct. Biol.* **2002**, *9*, 337–342.

The main limitation of our method is the amount of cells that can be analyzed in a given field of view. The density of traps in the current device is 3300 single-cell traps/mm². Using a 10 \times objective and CCD field smaller than the microscope field of view allowed at most ~30 isolated cells/field. This magnification and camera allowed sampling of the cell diameter with ~10 pixels. Maintaining this level of geometric sampling, but designing arrays wide enough to fill the field, and using a camera with a larger CCD would easily increase this number to ~200 cells/field of view. For this current preliminary work, this method sacrifices throughput (as compared to FC, for example) for spatial and temporal accuracy. To elaborate, although FC can interrogate hundreds of thousands of cells, and at several time points, analysis of the same cell over a long period of time is not possible, nor is positional-dependent analysis of fluorescence within individual cells. Particularly difficult to probe with FC is fast time-dependent changes upon addition of a compound to a cell. The device and techniques presented have the potential to bridge all of these gaps in FC, with moderate throughput.

CONCLUSIONS

The experiments and methods presented here are expected to have a large impact on high-throughput experimentation with single cells because of the robust nature of the device and the ease of operation. The intent was to allow the technology to be accessible to biologists not specialized in working with microfluidic or other microfabricated devices. Encouraging on this front, the device has been successfully molded and operated after minimal training by five other colleagues not including the first author of this paper. Immediately, analysis of enzyme content and enzyme profiling of different cell types using a variety of fluorogenic substrates is possible.

ACKNOWLEDGMENT

This research was supported by a Whitaker Foundation graduate fellowship (D.D.), as well as GlaxoSmithKline and Intel. All molds were fabricated in the UC Berkeley microfabrication facility. The authors thank Paul J. Hung for key discussions and fabrication assistance.

SUPPORTING INFORMATION AVAILABLE

Additional information as noted in text. This material is available free of charge via the Internet at <http://pubs.acs.org>.

Received for review March 24, 2006. Accepted April 26, 2006.

AC060541S